Geophysical Research Letters

RESEARCH LETTER
10.1029/2021GL094693

Fate of Warm Pacific Water in the Arctic Basin

Peigen Lin[1], Robert S. Pickart[1], Kjetil Våge[2], and Jianqiang Li[3]

[1]Woods Hole Oceanographic Institution, Woods Hole, MA, USA, [2]University of Bergen and Bjerknes Centre for Climate Research, Geophysical Institute, Bergen, Norway, [3]State Key Laboratory of Marine Environmental Science, College of Ocean and Earth Sciences, Xiamen University, Xiamen, China

Key Points:

- Outflow of Pacific Summer Water (PSW) through Barrow Canyon is dictated predominantly by the local wind
- The westward flow carrying the water away from the canyon bifurcates downstream, modulated by the strength and extent of the Beaufort Gyre
- The eastward flow emanating from the canyon progresses far downstream, but the signature of the PSW is limited

Supporting Information:

Supporting Information may be found in the online version of this article.

Correspondence to:

P. Lin,
plinwhoi@gmail.com

Citation:

Lin, P., Pickart, R. S., Våge, K., & Li, J. (2021). Fate of warm Pacific water in the Arctic basin. *Geophysical Research Letters*, *48*, e2021GL094693. https://doi.org/10.1029/2021GL094693

Received 8 JUN 2021
Accepted 7 SEP 2021

Abstract Pacific Summer Water (PSW) plays a critical role in the ecosystem of the western Arctic Ocean, impacting sea-ice melt and providing freshwater to the basin. Most of the water exits the Chukchi Sea shelf through Barrow Canyon, but the manner in which this occurs and the ultimate fate of the water remain uncertain. Using an extensive collection of historical hydrographic and velocity data, we demonstrate how the PSW outflow depends on different wind conditions, dictating whether the warm water progresses eastward or westward away from the canyon. The current carrying the water westward along the continental slope splits into different branches, influenced by the strength and extent of the Beaufort Gyre, while the eastward penetration of PSW along the shelfbreak is limited. Our results provide the first broad-scale view of how PSW is transferred from the shelf to the basin, highlighting the role of winds, boundary currents, and eddy exchange.

Plain Language Summary Warm Pacific water that flows northward through Bering Strait significantly influences the melting of sea-ice, the distribution of freshwater, and the ecosystem of the Arctic Ocean. North of Bering Strait, the water progresses poleward across the shallow Chukchi Sea shelf, with most of it draining from the shelf through Barrow Canyon. Presently, the manner in which the flow exits the canyon, as well as its ultimate fate in the basin, remains unclear. We analyzed historical data sets of temperature, salinity, and velocity, and found that the local wind alters the manner in which the water exits Barrow Canyon to the east and west, as well as the corresponding distribution of Pacific Summer Water. The current carrying the water westward along the continental slope subsequently splits into different branches farther downstream. This is modulated by the strength and extent of the Beaufort Gyre, a large recirculating flow in the basin. In contrast, the signature of the warm water in the current flowing to the east is limited. Here, we provide the first observational broad-scale view of the pathways and evolution of warm Pacific-origin water from the shelf to the basin, and clarify the effects of wind, boundary currents, and small-scale turbulent motions.

1. Introduction

Pacific water that flows through Bering Strait into the Chukchi Sea is the predominant source of freshwater, heat, and nutrients that strongly impact the halocline, ice conditions, and ecosystem of the western Arctic Ocean (Shimada et al., 2006; Steele et al., 2004; Woodgate et al., 2010). North of the strait the water progresses poleward across the Chukchi shelf mainly via three pathways (Figure 1): the western pathway through Herald Canyon, the Central Channel pathway, and the Alaskan Coastal Current (ACC; Lin, Pickart, McRaven, et al., 2019; Paquette & Bourke, 1979; Pickart et al., 2010). Ultimately, a large percentage of the Pacific water drains from the shelf via Barrow Canyon, particularly in summer (Gong & Pickart, 2015; Itoh et al., 2013, 2015). Exiting Barrow Canyon, some of the outflows forms an eastward-flowing current to the Beaufort Sea, known as the Beaufort Shelfbreak Jet (Figure 1; Nikolopoulos et al., 2009; Pickart, 2004), while the majority of the outflow feeds the westward-flowing Chukchi Slope Current (Figure 1). The existence and variability of the Chukchi Slope Current has been confirmed observationally through a combination of shipboard sections, moorings, surface drifters, and profiling floats (Corlett & Pickart, 2017; Li et al., 2019; Stabeno et al., 2018; Stabeno & McCabe, 2020). The dynamics of the current were investigated in an idealized numerical study, where it was argued that the westward flow originating from the canyon arises due to the sea surface height (SSH) slope associated with the Beaufort Gyre (Spall et al., 2018; Figure 1).

More recent work has indicated that the Chukchi Slope Current does not arise entirely from the outflow from Barrow Canyon, but is also fed by westward flow emanating from the Beaufort slope. This is evident

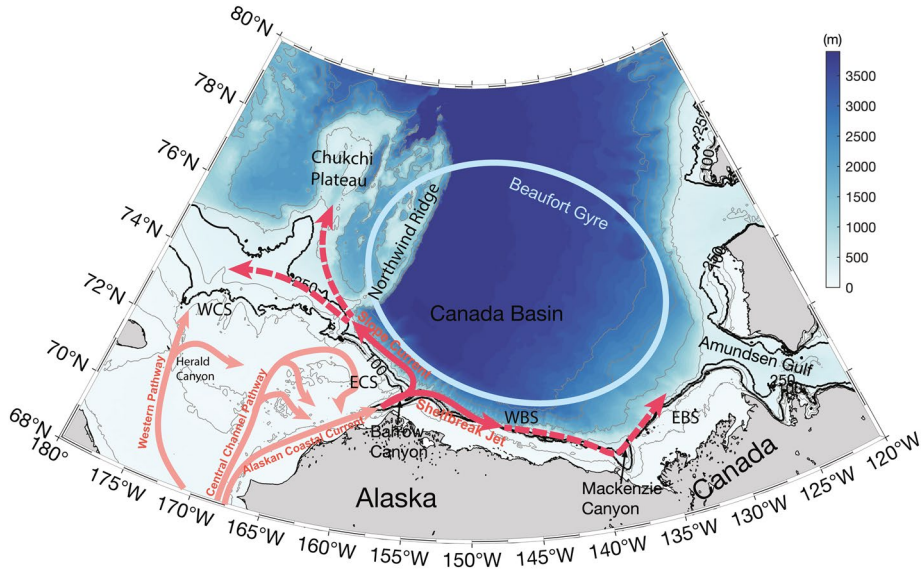

Figure 1. Schematic circulation of the western Arctic Ocean and place names. The main flow pathways of Pacific water across the Chukchi shelf are shown by the light red arrows. The Barrow Canyon outflow, Beaufort Shelfbreak Jet, and Chukchi Slope Current are marked by the red arrows, where the dashed portions indicate less certainty. The schematic Beaufort Gyre is marked by the light blue circle. WCS: western Chukchi Sea; ECS: eastern Chukchi Sea; WBS: western Beaufort Sea; EBS: eastern Beaufort Sea. The bathymetry (shaded and light black contours) is from IBCAO v3.

from a mass balance perspective (Stabeno & McCabe, 2020) and also from numerical modeling (Watanabe et al., 2017). A recent numerical simulation estimated that 62% of the Pacific water transport in the Chukchi Slope Current originates from the Barrow Canyon outflow, while the offshore westward jet from the Beaufort slope supplies the remaining 38% (Leng et al., 2021).

Away from Barrow Canyon, Lagrangian observations indicate that, after crossing the Northwind Ridge, the Chukchi Slope Current either flows westward along the continental slope (Stabeno & McCabe, 2020) or turns to the north (Boury et al., 2020). The recent model study of Leng et al. (2021) suggests that both of these fates are possible. With regard to the Beaufort Shelfbreak Jet, only a small number of the surface drifters launched on the Chukchi shelf entered the Beaufort Sea after exiting Barrow Canyon (Stabeno & McCabe, 2020). Mooring data indicate that the jet extends to the eastern Beaufort Sea (Forest et al., 2015; Lin et al., 2020), but an energetics analysis suggests that the summertime configuration of the current should spin down before reaching the Amundsen Gulf, the first entrance to the Canadian Arctic Archipelago (von Appen & Pickart, 2012). At this point, there remains considerable uncertainty regarding the fate of the Pacific water in both the Beaufort Shelfbreak Jet and the Chukchi Slope Current.

This study uses an extensive collection of historical hydrographic and velocity data to investigate the evolution of the Pacific Summer Water (PSW) exiting Barrow Canyon and its connection to the Chukchi Slope Current and Beaufort Shelfbreak Jet. We further aim to elucidate the downstream fate of the water. Our results indicate that variations in both the local wind and the Beaufort Gyre influence the water mass evolution and different kinematic pathways. We first investigate the evolution and forcing of PSW in the vicinity of Barrow Canyon, and then address the fate of the water farther downstream and the potential mechanisms dictating this fate.

2. Data and Methods

2.1. Historical Hydrographic Profiles

We use historical hydrographic data obtained from multiple data sources: (a) The Unified Database for Arctic and Subarctic Hydrography, which is a collection of temperature and salinity profiles for the period 1980–2015 (Behrendt et al., 2018); (b) The World Ocean Database 2018 (WOD18), provided by the National

Centers for Environmental Information, covering 1849–2020 in the domain of interest; (c) A composite data set of hydrographic observations in the Chukchi Sea spanning 1922–2019 (Danielson et al., 2020); and (d) Recent shipboard measurements from the Arctic Data Center that have not yet been added to the data sets above, which enhance the hydrographic coverage in the Beaufort Sea. The spatial and temporal coverage of the composite data set is shown in Figure S1a in Supporting Information S1. We consider the warm months from June to October over the time period 1970–2019, and have removed all duplicate profiles (Figures S1a and S1b in Supporting Information S1). The data consist primarily of conductivity-temperature-depth profiles from ships, ice-tethered profilers, and gliders. Some of the earlier measurements are bottle casts.

2.2. Historical Velocity

We have compiled shipboard acoustic Doppler current profiler data from 47 cruises that cover the Chukchi Sea and western Beaufort Sea from 2002 to 2018, during the warm months from June to October (Figures S1c and S1d in Supporting Information S1). The data have been subject to a rigorous quality control, and the barotropic tidal signal has been removed from each profile (see Text S1 in Supporting Information S1 for details).

2.3. Wind Product

The time series of 10 m winds from the meteorological station in Utqiaġvik, AK was obtained from the National Climate Data Center of the National Oceanic and Atmosphere Administration for the period 1970–2019. The data were subsequently edited to remove outliers, interpolate over small gaps, and put on an hourly time base following previous methodology (Pickart et al., 2013). This product has been widely used in previous regional studies (Pickart et al., 2019; Pisareva et al., 2019). Although atmospheric reanalysis fields provide broader coverage over the region, the Utqiaġvik wind data are not assimilated into these products, which motivates us to use the measured meteorological data (We show in Text S2 in Supporting Information S1 that the along-canyon wind from the ERA5 reanalysis is significantly correlated with the Utqiaġvik time series).

2.4. Sea Surface Height

We make use of the monthly altimetry-derived SSH product spanning the time period 2003–2014 (Armitage et al., 2016). The SSH data set is the combination of the estimation from sea ice openings in ice-covered regions and direct satellite measurements in ice-free regions. The data set has a spatial resolution of 0.75° × 0.25° in longitude and latitude, respectively, and extends to 81.5°N. The SSH gradient was computed as $\sqrt{\left(\partial \mathrm{SSH}/\partial x\right)^2 + \left(\partial \mathrm{SSH}/\partial y\right)^2}$.

2.5. Water Mass Analysis

Pacific-origin water consists of PSW and Pacific Winter Water (PWW; Gong & Pickart, 2016; Lin, Pickart, McRaven, et al., 2019; Weingartner et al., 1998). Besides these, the fresh water commonly found in the surface layer largely derives from sea ice melt and river water. Sometimes these are considered as a single water type, referred to as melt water/river runoff (MWR), when there are no means to distinguish them (Lin et al., 2016). The MWR can be very cold in the early season (MWR-cold) or quite warm in the late season (MWR-warm; Gong & Pickart, 2016). We cast the hydrographic data in potential density/potential spicity (σ/π) space (see Text S3 and Figure S2 in Supporting Information S1), where the potential density and potential spicity are referenced to the sea surface (Huang et al., 2018). In this framework, the MWR-warm and MWR-cold essentially collapse to a single σ/π value, which we refer to as MWR (Figure S2 in Supporting Information S1). This allows us to consider a mixing triangle of three end members, PSW, PWW, and MWR, that delimits nearly all of the data (the exception being a small amount of Atlantic Water that has been upwelled onto the Chukchi/Beaufort shelves). By assuming a linear mixture of these three end members, we then compute corresponding percentages of the end member water masses for each given water parcel.

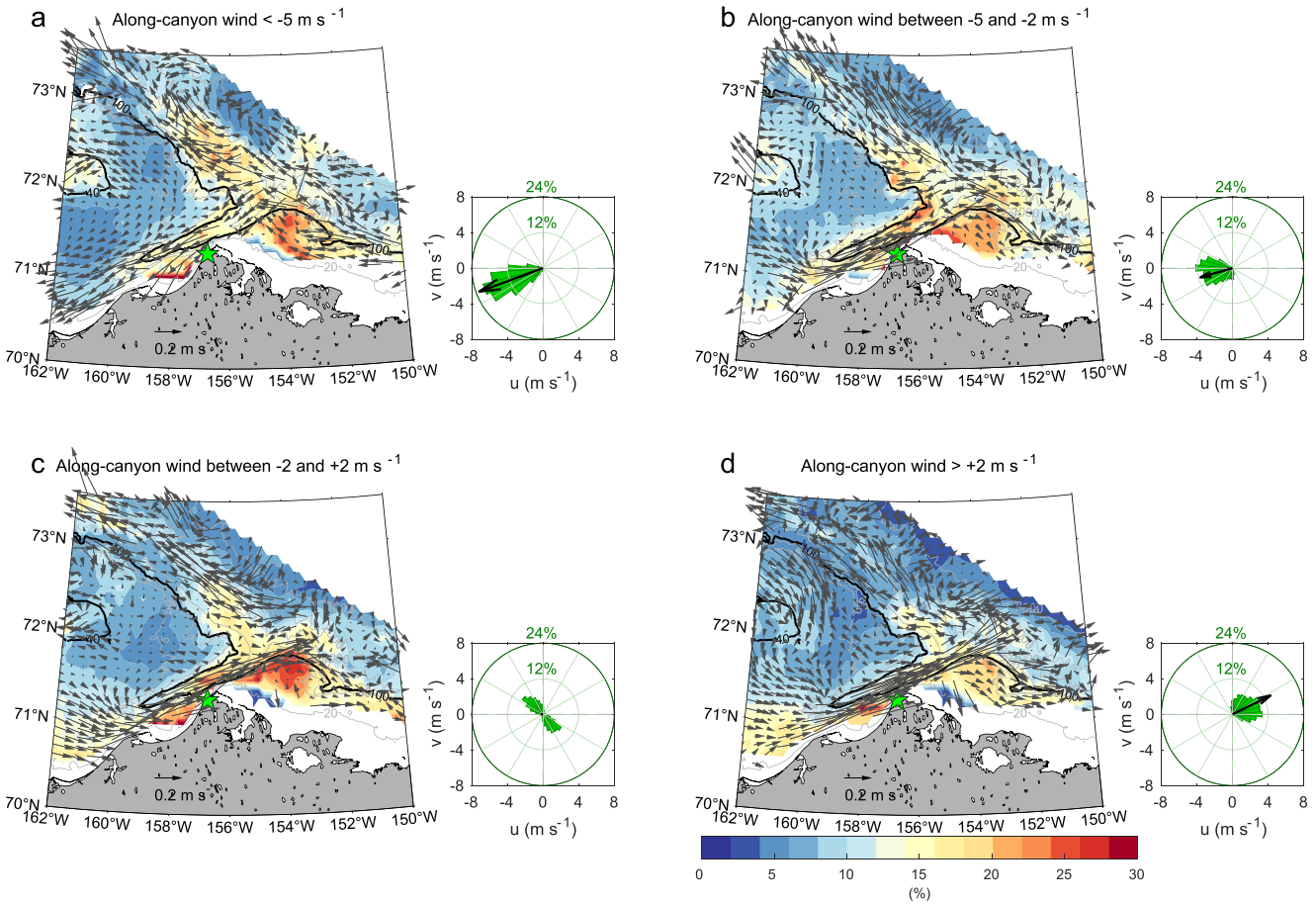

Figure 2. Composite velocity and PSW percentage maps for the four wind regimes. (a) Along-canyon wind <-5 m s^{-1}, (b) -5 to -2 m s^{-1}, (c) -2 to 2 m s^{-1}, (d) >2 m s^{-1}. The vectors are the vertically averaged velocity in the upper 100 m and the colors denote the PSW percentage at 30 m. The 40 and 100 m isobaths are highlighted by thick lines. The wind rose and mean wind vector for each scenario are computed using data from the Utqiaġvik weather station (green star on the map).

3. Outflow of Pacific Summer Water From Barrow Canyon

Previous studies have demonstrated that the Barrow Canyon outflow is strongly modulated by the along-canyon wind (Okkonen et al., 2009; Weingartner et al., 2017). Using mooring data from the canyon, together with the wind time series from the meteorological station in nearby Utqiaġvik, an empirical orthogonal function analysis demonstrates that the local wind is the dominant driver of the flow variability (see Text S4 in Supporting Information S1). As such, we consider four along-canyon wind regimes, where the along-canyon direction is 52°T (Pisareva et al., 2019). Using the historical data sets of hydrography and directly measured velocity described above, we created a composite map for each wind regime of vertically averaged velocity in the upper-100 m as well as the percentage of PSW at 30 m (in the middle of the PSW layer, elaborated on below). The lag times of the velocity (6 h) and hydrographic response (15 h) to wind are taken into account in the composites (see Text S5 in Supporting Information S1). Figure 2 shows the composites for each regime, encompassing the months of June–October (dictated by the seasonal coverage of the hydrographic and velocity data sets).

Regime 1: Along-canyon wind <-5 m s^{-1}. Under these conditions, the Barrow Canyon outflow, along with the ACC south of the canyon, are reversed by the strong northeasterly wind (Figure 2a). This reversal has also been noted in previous studies (Lin, Pickart, McRaven, et al., 2019; Pisareva et al., 2019). Since this wind direction also favors upwelling along the Beaufort slope, the Beaufort Shelfbreak Jet is also reversed to the west (Lin et al., 2016; Nikolopoulos et al., 2009). The reversed shelfbreak jet bifurcates at the mouth of Barrow Canyon, with part of the flow turning up-canyon to feed the reversed ACC, while the remaining

portion continues to the west and feeds the Chukchi Slope Current. Evidence of the latter westward flow is also seen in model studies (Leng et al., 2021; Watanabe et al., 2017). Unlike the other two water masses (PWW and MWR) that reside throughout the domain of Figure 2, the PSW presents a clear pathway from the Chukchi shelf to the basin, hence it is an appropriate tracer. One sees that, even though the outflow has been reversed, a PSW signal is present in the Chukchi Slope Current. In this case, the PSW is supplied by the westward flow from Beaufort Sea. This is consistent with the analysis of a synoptic easterly wind event using shipboard data and satellite SST imagery (Brugler et al., 2014). Importantly, the PSW in the Beaufort Sea initially came from the Barrow Canyon outflow via the eastward-flowing shelfbreak jet under different wind conditions (see below).

Regime 2: Along-canyon wind ranging from −5 to −2 m s^{-1}. Under the weakened northeasterly wind, the outflow from Barrow Canyon is re-established, but the offshore portion of the Beaufort Shelfbreak Jet is still reversed (Figure 2b). As these flows encounter each other these results in a chaotic flow structure close to the mouth of the canyon. Despite this, there is still a robust signature of PSW in the Chukchi Slope Current. Part of this signal stems from the westward flow coming from the Beaufort Sea (as was the case in the previous wind regime), but the largest signature is inshore of this (close to the shelfbreak) emanating from the canyon outflow.

Regime 3: Along-canyon wind ranging from −2 to 2 m s^{-1}. When the along-canyon component of the wind is weak or absent, the Barrow Canyon outflow and Beaufort Shelfbreak Jet are substantially intensified (Figure 2c). The strong outflow extends partly into the basin and then recirculates back to the slope on the west side of the canyon. As the warm water exits the canyon it likely mixes with colder water in the basin. This results in a weaker signal of PSW in the slope current. As seen in Figure 2c, while the along-canyon component of the wind is weak in this regime, the cross-canyon component displays a bimodal distribution—either from the southeast or northwest. In the former case, the PSW signal in the slope current is stronger, while in the latter case it is nearly absent (Text S6 and Figure S3 in Supporting Information S1).

Regime 4: Along-canyon wind >2 m s^{-1}. As the down-canyon wind strengthens more, the outflow is further intensified (up to 0.65 m s^{-1}) and penetrates even farther into the basin (Figure 2d). This essentially removes any direct connection with the Chukchi Slope Current close to the canyon mouth. Together with increased mixing with the cold water north of Barrow Canyon, this weakens the PSW signal in the slope current even further. In both this regime and the previous one, the outflow from Barrow Canyon feeds the Beaufort Shelfbreak Jet to the east, carrying with it a strong signature of PSW. This is the source of PSW that enters the slope current when the shelfbreak jet reverses under northeasterly winds (Regimes 1 and 2).

These results demonstrate that the Chukchi Slope Current is present during all of the wind regimes during the warm months of the year, and carries with it a signature of PSW. Upon first glance, however, the amount of warm water in the current seems counterintuitive. Since the source of the PSW is the Chukchi shelf (i.e., the ACC), one might expect that, under weak or reversed flow in Barrow Canyon, there would be a reduced PSW signature in the slope current. Instead, the opposite is true: as seen in Figure 2, as the along-canyon winds go from up-canyon to down-canyon, the PSW signal in the slope current gets progressively weaker. This is large because the outflow from the canyon extends farther into the basin with increasing down-canyon winds, allowing it to mix more readily with cold waters from the basin.

The above-mentioned model study of Leng et al. (2021) argues that the Chukchi Slope Current is fed by a combination of the outflow from Barrow Canyon (62% contribution) and a westward current extending from the Beaufort slope (38% contribution). Our composite maps in Figure 2 imply that this partitioning varies in time depending on the local wind conditions. In particular, westward flow from the Beaufort slope feeds the slope current only in the first two regimes corresponding to northeasterly winds (Figures 2a and 2b). It has been suggested that this flow emanates from the southern arm of the Beaufort Gyre (Leng et al., 2021), whereas as our water mass composites indicate that at least part of it emanates from Barrow Canyon, flows eastward into the Beaufort Sea, and then reverses to feed the slope current when the winds are northeasterly. Both of these scenarios could be at play; indeed, some of the westward flow in our composites (particularly in Regime 1) contains little to no PSW.

Note that PSW accumulates on the eastern flank of the canyon mouth in all four regimes. For Regimes 2–4, this may be related to the interaction of the eastward-turning outflow from the canyon and the widened

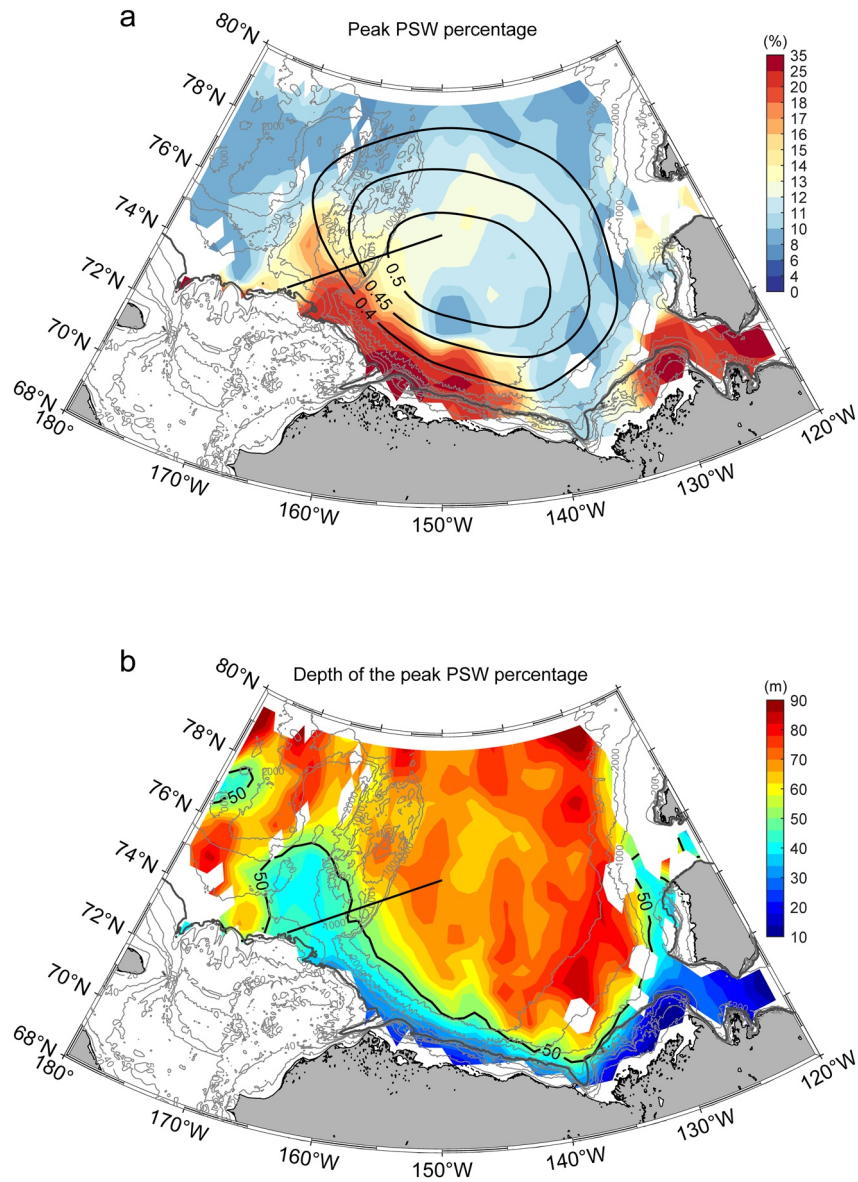

Figure 3. Lateral distribution of PSW in the Canada Basin. (a) The peak PSW percentage in the vertical, and (b) The corresponding depth at which the peak occurs. The data on the Chukchi shelf are not shown. In panel (a) the contours are the mean SSH contours of the Beaufort Gyre, and in panel (b) the 50 m PSW depth is contoured. The straight line is that presented in Figure 4.

shelf that forms a convergent zone (Pringle, 2002). Additionally, in Regime 1 when the Beaufort Shelfbreak Jet is reversed, the PSW is advected back toward the mouth and can again accumulate where the shelf widens, east of Barrow Canyon.

4. Evolution and Fate of the Pacific Summer Water

We now investigate the far-field signature of the PSW away from Barrow Canyon in both the Chukchi and Beaufort Seas.

Using the historical hydrographic data, we constructed a lateral map of the peak PSW percentage in the water column (Figure 3a). In particular, at each point in the domain, we tabulated the maximum value of the percentage in the vertical. The corresponding depth at which this occurs is mapped in Figure 3b. The PSW

signature extends to the west along the Chukchi slope and then subsequently divides into three tongues. The first tongue remains along the upper slope progressing toward the East Siberian Sea, the second tongue veers to the north on the east side of the Chukchi Plateau, and the third tongue extends to the northeast into the basin. Included in Figure 3a are the mean absolute dynamic height contours of the Beaufort Gyre using the satellite SSH product (Armitage et al., 2016; see Section 2). One sees that the second PSW tongue extends along the edge of the gyre, while the third (weaker) tongue protrudes into the gyre emanating from the region where the gyre encounters the Northwind Ridge (see Figure 1 for place names).

Using a passive tracer in their high-resolution numerical model, Leng et al. (2021) demonstrated that the Chukchi Slope Current bifurcates after crossing the Northwind Ridge, with part of the flow remaining on the continental slope and the other part progressing northward within the Chukchi Plateau along the edge of the Beaufort Gyre. These two pathways correspond to the first two tongues of enhanced PSW percentage in Figure 3a. In situ Lagrangian measurements support this scenario as well: surface drifters have identified the slope pathway (Stabeno & McCabe, 2020), while profiling SOLO floats have revealed the Chukchi Plateau pathway adjacent to the gyre (Boury et al., 2020). The depth of the largest PSW signal in the continental slope and Chukchi Plateau tongues (at least initially) is near 30 m (Figure 3b).

The third tongue of enhanced PSW percentage in Figure 3a spirals into the Beaufort Gyre at a deeper depth horizon (Figure 3b). It is consistent with the evidence presented in a model study (Hu & Myers, 2013), but has not been identified observationally before. The PSW comprising this tongue is likely being fluxed offshore by eddies which cause exchange between the boundary and interior (Spall et al., 2008). The strength of the tongue implies that this mechanism is less effective than the two advective pathways resulting in the other two tongues. Using the historical hydrographic data, we created a composite vertical section of PSW percentage extending from the upper continental slope, across the Chukchi Plateau tongue, and then along the interior PSW tongue that extends into the basin (the line is shown in Figure 4a, and is also indicated in Figure 3). On the slope, the PSW percentage is relatively high (>25%) in the depth range of 15–35 m (Figure 4b). The PSW percentage decreases toward the basin, while at the same time its core depth steadily deepens along isopycnals, indicative of subduction into the gyre.

We now address time variation in the penetration of PSW into the interior and its relationship to the state of the Beaufort Gyre. This was done by dividing the composite line in Figure 4a into four 120 km segments, starting at its southwest end. Then, for each segment we identified the hydrographic profiles within the segment with PSW percentage higher than 15%, tabulating the times of these profiles. Next, we constructed a SSH composite for the months corresponding to the selected profiles. We note that the SSH data have monthly resolution, while the hydrographic profiles in the database can correspond to any particular day. Hence, a given monthly SSH data point can appear in more than one of the segment composites. That said, the largest number of SSH realizations corresponded to the segment in question.

The lowest closed SSH contour around the peak is often used to define the edge of the Beaufort Gyre (Regan et al., 2019). While this represents the gyre extent, the gyre intensity is also dynamically important. In order to consider both, for each composite, we considered the same SSH contour, 0.45 m, along with the maximum SSH gradient. This reveals a relationship between the amount of PSW in each segment and the extent and strength of the gyre. In particular, enhanced amounts of PSW (higher than 15%) are found farther offshore as the gyre contracts and weakens (Figure 4c). This is consistent in that, as the advective speed of the gyre decreases, the eddies are more apt to carry PSW into the gyre. Our results thus imply that the path of the Chukchi Slope Current is dynamically tied to the extent and strength of the Beaufort Gyre. Since the gyre expanded from 2003 to 2014 (Regan et al., 2019), this suggests that more PSW flowed toward the west instead of protruding into the gyre during this time period.

Considering now the Beaufort Sea, one sees that the PSW signal along the boundary decreases markedly as it reaches the Canadian Beaufort Sea (Figure 3a), in line with the hypothesis of von Appen and Pickart (2012). Note that east of 135°W the value increases again, such that in the vicinity of Amundsen Gulf the PSW percentage is as high as the initial value in the Barrow Canyon. This is likely a local signal arising from mixing of warm, fresh sea-ice melt water and cold, salty winter water (the mixing line between the MWR-warm and PWW end-members passes through this part of the θ/S plane, Figure S2a in Supporting Information S1). This is line with the previous water mass analysis of Forest et al. (2015). Note that the depth

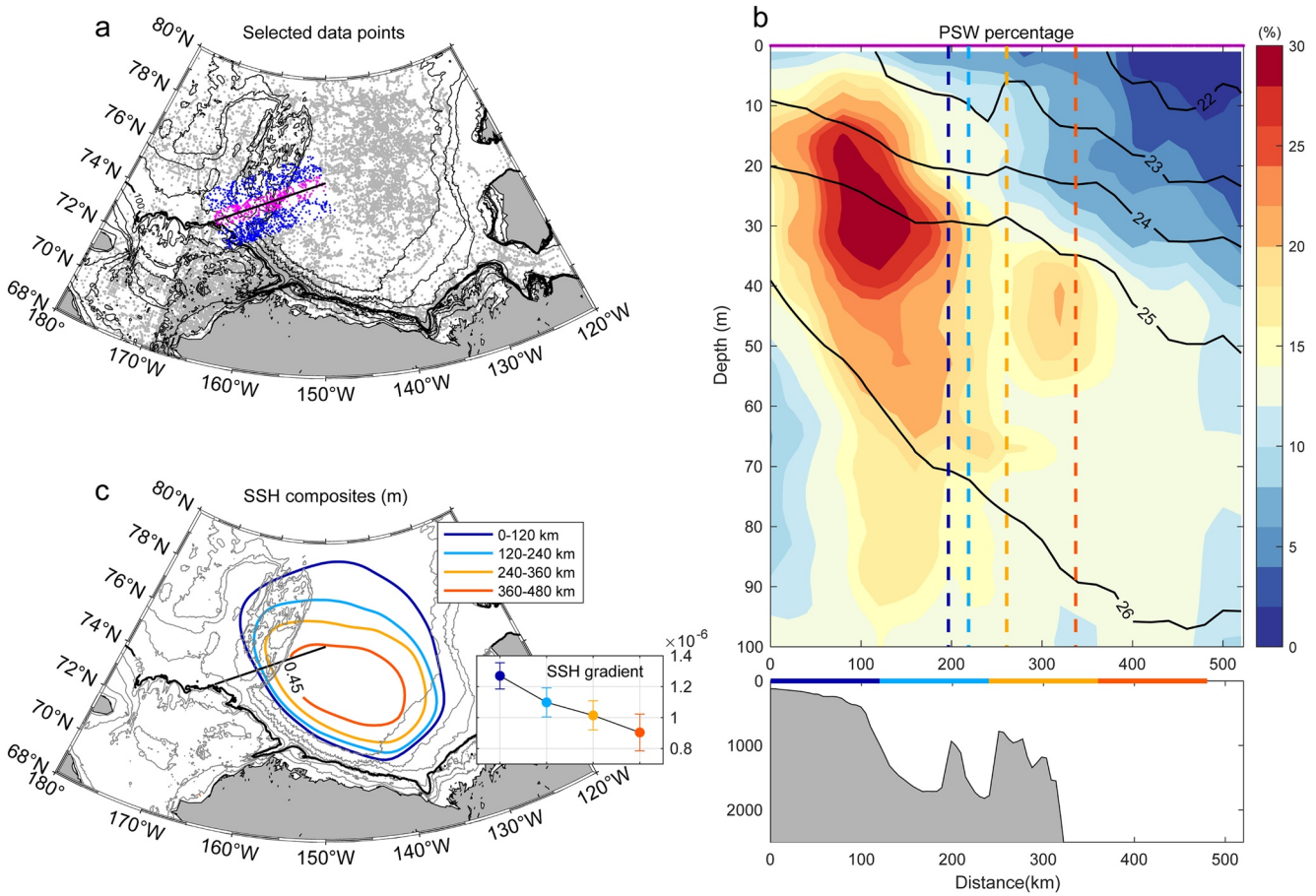

Figure 4. PSW in relation to the Beaufort Gyre. (a) Locations of the selected profiles (colored dots) projected onto the solid line used to create the mean section in panel (b) and for guiding the construction of the SSH composites in panel (c). The bathymetry is from IBCAO v3 (black contours). The 100 m isobath is highlighted. (b) The mean section of PSW percentage along the section using the magenta-colored data points in panel (a). The data coverage is marked on the top. The top panel shows the upper 100 m of the section, with the associated bathymetry shown in the bottom panel. The colored lines along the bottom panel denote the four 120 km segments used for constructing the sea surface height (SSH) composites discussed in the text. The vertical dashed lines in the top panel denote the intersection of the line in panel (a) with the Beaufort Gyre isoline in each composite in panel (c) (using the same color scheme). (c) The 0.45 m isoline of SSH for the four composites and the corresponding SSH gradient (same color scheme), using the blue and magenta data profiles in panel (a).

of the signal near Amundsen Gulf is much shallower (~15 m, Figure 3b), which suggests that summertime atmospheric heating may also be playing a role. Our interpretation of this eastern signal is consistent with the fact that only a very small amount of PSW was found in the vicinity of Mackenzie Canyon based on mooring data (Lin et al., 2020).

To further elucidate the nature of the PSW signal away from Barrow Canyon, we constructed a vertical section of PSW percentage along the 250 m isobath (Figure 5). The outflow of PSW from the canyon is evident throughout the upper 100 m and peaks near 30 m (Figure 5b). This is consistent with the fine-scale observations of MacKinnon et al. (2021) showing a PSW wedge that intrudes into the basin with maximum signal in the subsurface. Figure 5 indicates that the PSW core remains centered near 30 m as it progresses westward along the Chukchi continental slope. By contrast, the high PSW signal deepens as it extends eastward toward the middle of the western Beaufort Sea (the isolated signal at shallow depth near the mouth of Amundsen Gulf is evident, although smaller than in Figure 3 because the 250 m isobath is offshore of the largest signal).

What causes the loss of the PSW signal away from Barrow Canyon? To investigate this, we tabulated the percentages of the other two water masses (PWW and MWR) along the 250 m isobath at two different depths, 5 and 30 m. These, along with the PSW percentage, are presented in Figures 5c and 5d as anomalies from the Barrow Canyon outflow location. At 5 m, the PSW decrease owes equally to an increase of PWW

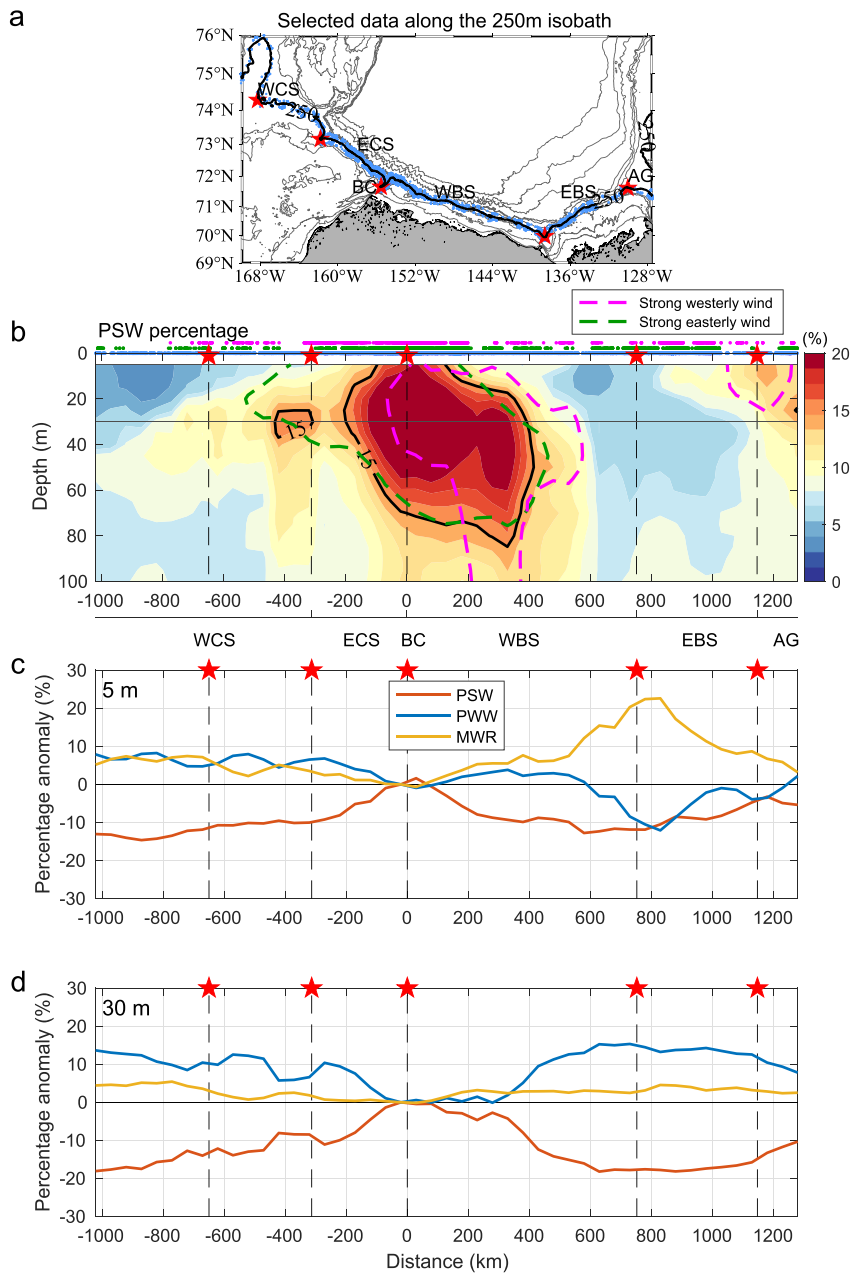

Figure 5. PSW presence along the continental slope. (a) Locations of the selected data (blue dots) along the 250 m isobath. The red stars denote select locations along the section for reference. (b) The vertical section of the PSW percentage along the 250 m isobath, overlain by the composite contours of 15% PSW percentage for the strong westerly wind (>5.5 m s^{-1}) and easterly wind (<−5.5 m s^{-1}) periods (see legend). The data coverage for each composite is marked on the top. (c, d) The percentage anomalies of PSW (red), PWW (blue), MWR (yellow) relative to the values at Barrow Canyon, along the 250 m isobath at 5 and 30 m, respectively. The location of Barrow Canyon corresponds to 0 km, positive (negative) distance is eastward (westward). WCS, western Chukchi Sea; ECS, eastern Chukchi Sea; BC, Barrow Canyon, WBS, western Beaufort Sea; EBS, eastern Beaufort Sea; AG, Amundsen Gulf.

and MWR on the Chukchi slope, while it is mainly due to a substantial increase of MWR on the Beaufort slope (Figure 5c), particularly in the region near the Mackenzie River plume (750–800 km). By contrast, at 30 m PWW plays the dominant role in displacing the PSW on the both sides of Barrow Canyon (Figure 5d).

It is well known that the Beaufort Shelfbreak Jet is intensified under westerly wind and weakened or reversed under strong easterly wind (Foukal et al., 2019; Lin, Pickart, Moore, et al., 2019; Lin et al., 2016).

Furthermore, the westward-flowing Chukchi Slope Current is enhanced when the winds are strongly out of the east (Corlett & Pickart, 2017; Li et al., 2019). As such, the local wind can also be a candidate for modifying the PSW signal along the continental slope. We, therefore, constructed an analogous vertical section of PSW percentage to that of Figure 5b, except using only the profiles when there are strong easterly winds (<-5.5 m s^{-1}, close to the peak wind speed for the mean upwelling in the western Beaufort Sea (Lin, Pickart, Moore, et al., 2019)), and a second analogous vertical section corresponding to strong westerly winds (>5.5 m s^{-1}, strong enough to enhance the Beaufort Shelfbreak Jet (Foukal et al., 2019)), respectively. The lag in the water column response to the wind was again taken into account.

Comparing the 15% contour (colored dashed lines in Figure 5b), one sees that when the wind blows strongly from the west, most of the PSW turns to the right upon exiting Barrow Canyon. In this condition, the PSW front extends roughly 150 km farther to the east, nearing the eastern Beaufort Sea, due to the intensified shelfbreak jet. The PSW signal also extends deeper in the water column (exceeding 100 m), likely due to the occurrence of shelfbreak downwelling under westerly winds (Foukal et al., 2019). The small PSW percentage to the west of Barrow Canyon is because of the mixing with ambient water for the strong canyon outflow scenario discussed above. During strong easterly winds, the location of the PSW front in the Beaufort Sea is close to the mean, while the signal extends much farther to the west along the Chukchi continental slope, in concert with the enhanced slope current. Thus, while the slope current is dynamically linked to the Beaufort Gyre in the basin as demonstrated earlier, the local wind also modifies the current and the PSW extension in the upper layer.

5. Conclusions

Using composite data sets of hydrography and directly measured velocity, we have shown how PSW outflows from Barrow Canyon and subsequently feeds the Chukchi Slope Current to the west and the Beaufort Shelfbreak Jet to the east. The outflow and partitioning of the PSW is dictated by the along-canyon winds. Under southwesterly wind the outflow from Barrow Canyon is strong and mixes with ambient water in the basin, leading to lower amounts of PSW entering the slope current. Under northeasterly wind, water from the Beaufort slope supplies the slope current with relatively high levels of recirculated PSW. Downstream, the slope current bifurcates with a tongue of PSW extending along the Chukchi continental slope and a second tongue progressing northward along the edge of the Beaufort Gyre. A third PSW tongue spreads directly into the gyre along isopycnals, likely the result of eddy transfer. The penetration of PSW from the slope current into the interior is influenced by both the extent and strength of the Beaufort Gyre. To the east, the PSW signature in the Beaufort Shelfbreak Jet largely vanishes before reaching the Canadian Beaufort Sea due to the lateral barrier of the PWW and MWR, although its penetration is modified by the local wind.

PSW is a critical component of the regional ecosystem, impacting sea-ice melt, influencing the vertical structure of the water column, and providing fresh water to the Beaufort Gyre. Our results provide the first broad-scale view of how PSW is transferred from the Chukchi shelf to the Pacific Arctic basin, highlighting the role of winds, boundary currents, and eddy exchange. Further work is required to understand what dictates the relative partitioning of the PSW downstream in the slope current—including its time dependence—and to quantify how this water mass ultimately ventilates the Beaufort Gyre.

Data Availability Statement

The historical hydrographic data are from the following sources. (a) the Unified Database for Arctic and Subarctic Hydrography (UDASH, https://doi.pangaea.de/10.1594/PANGAEA.872931). (b) World Ocean Database 2018 (WOD18, https://www.ncei.noaa.gov/products/world-ocean-database). (c) A compiled data set in the Chukchi Sea provided by S. Danielson with data from the following sources: WOD18; Pacific Marine Environmental Laboratory (PMEL, https://www.pmel.noaa.gov/epic/ewb/); NOAA Alaska Fisheries Science Center (https://data.eol.ucar.edu/dataset/); University of Alaska Fairbanks Institute of Marine Science (UAF IMS, available at the Arctic Ocean Observing System, http://www.aoos.org); Fisheries and Oceans Canada's Institute of Ocean Sciences (IOS, https://www.pac.dfo-mpo.gc.ca/science/index-eng.html); and Japan Agency for Marine-Earth Science and Technology (JAMSTEC, http://www.godac.jamstec.go.jp/darwin/e/). (d) The Arctic Observing Network (AON) hydrographic data from the Arctic Data Center

(https://arcticdata.io/catalog/data). The shipboard ADCP velocity data can be found at https://www.rvdata.us/search/vessel/Healy. Wind data from the meteorological station in Utqiaġvik, AK are available at https://www.ncdc.noaa.gov/cdo-web/datatools/findstation. Sea surface height data are available via http://www.cpom.ucl.ac.uk/dynamic_topography. ERA5 reanalysis data are obtained from the European Center for Medium-Range Weather Forecasts (ECMWF, https://rmets.onlinelibrary.wiley.com/doi/10.1002/qj.3803). The mooring data near the head of the Barrow Canyon is available at National Oceanographic Data Center (NODC, https://www.nodc.noaa.gov/archive/arc0113/0160090/). The mooring data at the mouth of the Barrow Canyon are published by JAMSTEC (http://www.jamstec.go.jp/arctic). The bathymetry data are from the International Bathymetric Chart of the Arctic Ocean (IBCAO) v3 (https://www.gebco.net/about_us/committees_and_groups/scrum/ibcao/ibcao_v3.html).

Acknowledgments
The authors acknowledge F. Bahr and L. McRaven for their contributions to the composite shipboard velocity dataset, and S. Danielson for providing access to a previously compiled hydrographic dataset. Much of the data from the Beaufort continental slope was collected as part of the Arctic Observing Network. Funding for the project was provided by National Science Foundation grant OPP-1733564 and National Oceanic and Atmospheric Administration grant NA14OAR4320158 (P. Lin, R. S. Pickart, J. Li), and Trond Mohn Foundation Grant BFS2016REK01 (K. Vage).

References

Armitage, T. W., Bacon, S., Ridout, A. L., Thomas, S. F., Aksenov, Y., & Wingham, D. J. (2016). Arctic sea surface height variability and change from satellite radar altimetry and GRACE, 2003–2014. *Journal of Geophysical Research: Oceans*, *121*(6), 4303–4322. https://doi.org/10.1002/2015jc011579

Behrendt, A., Sumata, H., Rabe, B., & Schauer, U. (2018). UDASH-Unified database for Arctic and subarctic hydrography. *Earth System Science Data*, *10*(2), 1119–1138. https://doi.org/10.5194/essd-10-1119-2018

Boury, S., Pickart, R. S., Odier, P., Lin, P., Li, M., Fine, E. C., et al. (2020). Whither the Chukchi Slope Current? *Journal of Physical Oceanography*, *50*(6), 1717–1732. https://doi.org/10.1175/jpo-d-19-0273.1

Brugler, E. T., Pickart, R. S., Moore, G. W. K., Roberts, S., Weingartner, T. J., & Statscewich, H. (2014). Seasonal to interannual variability of the Pacific water boundary current in the Beaufort Sea. *Progress in Oceanography*, *127*, 1–20. https://doi.org/10.1016/j.pocean.2014.05.002

Corlett, W. B., & Pickart, R. S. (2017). The Chukchi Slope Current. *Progress in Oceanography*, *153*, 50–65. https://doi.org/10.1016/j.pocean.2017.04.005

Danielson, S., Ahkinga, O., Ashjian, C., Basyuk, E., Cooper, L., Eisner, L., et al. (2020). Manifestation and consequences of warming and altered heat fluxes over the Bering and Chukchi Sea continental shelves. *Deep Sea Research Part II: Topical Studies in Oceanography*, *177*, 104781. https://doi.org/10.1016/j.dsr2.2020.104781

Forest, A., Osborne, P. D., Fortier, L., Sampei, M., & Lowings, M. G. (2015). Physical forcings and intense shelf-slope fluxes of particulate matter in the halocline waters of the Canadian Beaufort Sea during winter. *Continental Shelf Research*, *101*, 1–21. https://doi.org/10.1016/j.csr.2015.03.009

Foukal, N. P., Pickart, R. S., Moore, G., & Lin, P. (2019). Shelfbreak downwelling in the Alaskan Beaufort Sea. *Journal of Geophysical Research: Oceans*, *124*, 7201–7225. https://doi.org/10.1029/2019jc015520

Gong, D., & Pickart, R. S. (2015). Summertime circulation in the eastern Chukchi Sea. *Deep Sea Research Part II: Topical Studies in Oceanography*, *118*, 18–31. https://doi.org/10.1016/j.dsr2.2015.02.006

Gong, D., & Pickart, R. S. (2016). Early summer water mass transformation in the Eastern Chukchi Sea. *Deep Sea Research Part II: Topical Studies in Oceanography*, *130*, 43–55. https://doi.org/10.1016/j.dsr2.2016.04.015

Hu, X., & Myers, P. G. (2013). A Lagrangian view of Pacific water inflow pathways in the Arctic Ocean during model spin-up. *Ocean Modelling*, *71*, 66–80. https://doi.org/10.1016/j.ocemod.2013.06.007

Huang, R. X., Yu, L. S., & Zhou, S. Q. (2018). New definition of potential spicity by the least square method. *Journal of Geophysical Research: Oceans*, *123*(10), 7351–7365. https://doi.org/10.1029/2018jc014306

Itoh, M., Nishino, S., Kawaguchi, Y., & Kikuchi, T. (2013). Barrow Canyon volume, heat, and freshwater fluxes revealed by long-term mooring observations between 2000 and 2008. *Journal of Geophysical Research: Oceans*, *118*(9), 4363–4379. https://doi.org/10.1002/jgrc.20290

Itoh, M., Pickart, R. S., Kikuchi, T., Fukamachi, Y., Ohshima, K. I., Simizu, D., et al. (2015). Water properties, heat and volume fluxes of Pacific water in Barrow Canyon during summer 2010. *Deep Sea Research Part I: Oceanographic Research Papers*, *102*, 43–54. https://doi.org/10.1016/j.dsr.2015.04.004

Leng, H., Spall, M. A., Pickart, R. S., Lin, P., & Bai, X. (2021). Origin and fate of the Chukchi Slope Current using a numerical model and in situ data. *Journal of Geophysical Research: Oceans*, *126*, e2021JC017291. https://doi.org/10.1029/2021jc017291

Li, M., Pickart, R. S., Spall, M. A., Weingartner, T. J., Lin, P., Moore, G., & Qi, Y. (2019). Circulation of the Chukchi Sea shelfbreak and slope from moored time series. *Progress in Oceanography*, *172*, 14–33. https://doi.org/10.1016/j.pocean.2019.01.002

Lin, P., Pickart, R. S., Fissel, D., Ross, E., Kasper, J., Bahr, F., et al. (2020). Circulation in the vicinity of Mackenzie Canyon from a year-long mooring array. *Progress in Oceanography*, *187*, 102396. https://doi.org/10.1016/j.pocean.2020.102396

Lin, P., Pickart, R. S., McRaven, L. T., Arrigo, K. R., Bahr, F., Lowry, K. E., et al. (2019). Water mass evolution and circulation of the northeastern Chukchi Sea in summer: Implications for nutrient distributions. *Journal of Geophysical Research: Oceans*, *127*(7), 4416–4432. https://doi.org/10.1029/2019jc015185

Lin, P., Pickart, R. S., Moore, G. W. K., Spall, M. A., & Hu, J. (2019). Characteristics and dynamics of wind-driven upwelling in the Alaskan Beaufort Sea based on six years of mooring data. *Deep Sea Research Part II: Topical Studies in Oceanography*, *162*, 79–92. https://doi.org/10.1016/j.dsr2.2018.01.002

Lin, P., Pickart, R. S., Stafford, K. M., Moore, G., Torres, D. J., Bahr, F., & Hu, J. (2016). Seasonal variation of the Beaufort shelfbreak jet and its relationship to Arctic cetacean occurrence. *Journal of Geophysical Research: Oceans*, *121*(12), 8434–8454. https://doi.org/10.1002/2016jc011890

MacKinnon, J. A., Simmons, H. L., Hargrove, J., Thomson, J., Peacock, T., Alford, M. H., et al. (2021). A warm jet in a cold ocean. *Nature communications*, *12*(1), 2418. https://doi.org/10.1038/s41467-021-22505-5

Nikolopoulos, A., Pickart, R. S., Fratantoni, P. S., Shimada, K., Torres, D. J., & Jones, E. P. (2009). The western Arctic boundary current at 152°W: Structure, variability, and transport. *Deep Sea Research Part II: Topical Studies in Oceanography*, *56*(17), 1164–1181. https://doi.org/10.1016/j.dsr2.2008.10.014

Okkonen, S. R., Ashjian, C. J., Campbell, R. G., Maslowski, W., Clement-Kinney, J. L., & Potter, R. (2009). Intrusion of warm Bering/Chukchi waters onto the shelf in the western Beaufort Sea. *Journal of Geophysical Research: Oceans*, *114*(C1). https://doi.org/10.1029/2008jc004870

Paquette, R. G., & Bourke, R. H. (1979). Temperature fine structure near the sea-ice margin of the Chukchi Sea. *Journal of Geophysical Research: Oceans*, *84*(C3), 1155–1164. https://doi.org/10.1029/jc084ic03p01155

Pickart, R. S. (2004). Shelfbreak circulation in the Alaskan Beaufort Sea: Mean structure and variability. *Journal of Geophysical Research*, *109*(C4). https://doi.org/10.1029/2003jc001912

Pickart, R. S., Nobre, C., Lin, P., Arrigo, K. R., Ashjian, C. J., Berchok, C., et al. (2019). Seasonal to mesoscale variability of water masses and atmospheric conditions in Barrow Canyon, Chukchi Sea. *Deep Sea Research Part II: Topical Studies in Oceanography*. https://doi.org/10.1016/j.dsr2.2019.02.003

Pickart, R. S., Pratt, L. J., Torres, D. J., Whitledge, T. E., Proshutinsky, A. Y., Aagaard, K., et al. (2010). Evolution and dynamics of the flow-through Herald Canyon in the western Chukchi Sea. *Deep Sea Research Part II: Topical Studies in Oceanography*, *57*(1–2), 5–26. https://doi.org/10.1016/j.dsr2.2009.08.002

Pickart, R. S., Spall, M. A., & Mathis, J. T. (2013). Dynamics of upwelling in the Alaskan Beaufort Sea and associated shelf-basin fluxes. *Deep Sea Research Part I: Oceanographic Research Papers*, *76*, 35–51. https://doi.org/10.1016/j.dsr.2013.01.007

Pisareva, M. N., Pickart, R. S., Lin, P., Fratantoni, P. S., & Weingartner, T. J. (2019). On the nature of wind-forced upwelling in Barrow Canyon. *Deep Sea Research Part II: Topical Studies in Oceanography*.

Pringle, J. M. (2002). Enhancement of wind-driven upwelling and downwelling by alongshore bathymetric variability. *Journal of Physical Oceanography*, *32*(11), 3101–3112. https://doi.org/10.1175/1520-0485(2002)032<3101:eowdua>2.0.co;2

Regan, H. C., Lique, C., & Armitage, T. W. (2019). The Beaufort Gyre extent, shape, and location between 2003 and 2014 from satellite observations. *Journal of Geophysical Research: Oceans*, *124*(2), 844–862. https://doi.org/10.1029/2018jc014379

Shimada, K., Kamoshida, T., Itoh, M., Nishino, S., Carmack, E., McLaughlin, F., et al. (2006). Pacific Ocean inflow: Influence on catastrophic reduction of sea ice cover in the Arctic Ocean. *Geophysical Research Letters*, *33*(8). https://doi.org/10.1029/2005gl025624

Spall, M. A., Pickart, R. S., Fratantoni, P. S., & Plueddemann, A. J. (2008). Western Arctic shelfbreak eddies: Formation and transport. *Journal of Physical Oceanography*, *38*(8), 1644–1668. https://doi.org/10.1175/2007jpo3829.1

Spall, M. A., Pickart, R. S., Li, M., Itoh, M., Lin, P., Kikuchi, T., & Qi, Y. (2018). Transport of Pacific water into the Canada Basin and the formation of the Chukchi Slope Current. *Journal of Geophysical Research: Oceans*, *123*(10), 7453–7471. https://doi.org/10.1029/2018jc013825

Stabeno, P. J., Kachel, N., Ladd, C., & Woodgate, R. (2018). Flow patterns in the eastern Chukchi Sea: 2010–2015. *Journal of Geophysical Research: Oceans*, *123*(2), 1177–1195. https://doi.org/10.1002/2017jc013135

Stabeno, P. J., & McCabe, R. M. (2020). Vertical structure and temporal variability of currents over the Chukchi Sea continental slope. *Deep Sea Research Part II: Topical Studies in Oceanography*, *177*, 104805. https://doi.org/10.1016/j.dsr2.2020.104805

Steele, M., Morison, J., Ermold, W., Rigor, I., Ortmeyer, M., & Shimada, K. (2004). Circulation of summer Pacific halocline water in the Arctic Ocean. *Journal of Geophysical Research: Oceans*, *109*(C2). https://doi.org/10.1029/2003jc002009

von Appen, W.-J., & Pickart, R. S. (2012). Two configurations of the western Arctic shelfbreak current in summer. *Journal of Physical Oceanography*, *42*(3), 329–351. https://doi.org/10.1175/jpo-d-11-026.1

Watanabe, E., Onodera, J., Itoh, M., Nishino, S., & Kikuchi, T. (2017). Winter transport of subsurface warm water toward the Arctic Chukchi Borderland. *Deep Sea Research Part I: Oceanographic Research Papers*, *128*, 115–130. https://doi.org/10.1016/j.dsr.2017.08.009

Weingartner, T. J., Cavalieri, D. J., Aagaard, K., & Sasaki, Y. (1998). Circulation, dense water formation, and outflow on the northeast Chukchi shelf. *Journal of Geophysical Research: Oceans*, *103*(C4), 7647–7661. https://doi.org/10.1029/98jc00374

Weingartner, T. J., Potter, R. A., Stoudt, C. A., Dobbins, E. L., Statscewich, H., Winsor, P. R., et al. (2017). Transport and thermohaline variability in Barrow Canyon on the northeastern Chukchi Sea Shelf. *Journal of Geophysical Research: Oceans*, *122*(5), 3565–3585. https://doi.org/10.1002/2016jc012636

Woodgate, R. A., Weingartner, T., & Lindsay, R. (2010). The 2007 Bering Strait oceanic heat flux and anomalous Arctic sea-ice retreat. *Geophysical Research Letters*, *37*(1). https://doi.org/10.1029/2009gl041621

References From the Supporting Information

Davis, R. E. (1998). Preliminary results from directly measuring middepth circulation in the tropical and South Pacific. *Journal of Geophysical Research*, *103*(C11), 24619–24639. https://doi.org/10.1029/98jc01913

Gao, Y., Huang, R. X., Zhu, J., Huang, Y., & Hu, J. (2020). Using the sigma-Pi diagram to analyze water masses in the Northern South China Sea in spring. *Journal of Geophysical Research: Oceans*, Vol. *125*(7), e2019JC015676. https://doi.org/10.1029/2019jc015676

Hersbach, H. (2018). *Operational global reanalysis: Progress, future directions and synergies with NWP*. European Centre for Medium Range Weather Forecasts.

Huang, J., Pickart, R. S., Huang, R. X., Lin, P., Brakstad, A., & Xu, F. (2020). Sources and upstream pathways of the densest overflow water in the Nordic Seas. *Nature Communications*, *11*(1), 1–9. https://doi.org/10.1038/s41467-020-19050-y

Schulze, L. M., & Pickart, R. S. (2012). Seasonal variation of upwelling in the Alaskan Beaufort Sea: Impact of sea ice cover. *Journal of Geophysical Research*, *117*, C06022. https://doi.org/10.1029/2012jc007985

Smith, W., & Wessel, P. (1990). Gridding with continuous curvature splines in tension. *Geophysics*, *55*(3), 293–305. https://doi.org/10.1190/1.1442837

Våge, K., Pickart, R. S., Spall, M. A., Moore, G., Valdimarsson, H., Torres, D. J., et al. (2013). Revised circulation scheme north of the Denmark Strait. *Deep Sea Research Part I: Oceanographic Research Papers*, *79*, 20–39. https://doi.org/10.1016/j.dsr.2013.05.007